An Improved Altimetry Wet Tropospheric Correction Retrieval Over Coastal Regions for the Sentinel-3 Mission

Pedro Aguiar, Telmo Vieira, Clara Lázaro, and M. Joana Fernandes

***Abstract*—The wet tropospheric correction (WTC) retrieval over coastal regions is still nowadays a challenging task. The open-ocean retrieval algorithms, which rely on microwave radiometers (MWR) brightness temperatures (TBs) measurements, fail to provide accurate WTC values over these transition surfaces, due to the land contamination on the TBs. The retrieval errors rapidly increase with the approach of the satellite to the coastline. In this article, an improvement of the WTC retrieval over coastal regions for the Sentinel-3 mission is proposed, based on the dual-band MWR measurements, complemented with additional parameters to account for surface effects. Methods of modification of the MWR TBs and the synthetic aperture radar altimeter backscatter coefficient σ_0, at Ku band, are presented, which aim to mitigate land contamination effects. On a first phase, these modified inputs are used in the open-ocean retrieval algorithm to compute the WTC. On a second phase, the same modified inputs are used in developed WTC retrieval algorithms specifically trained in coastal regions. The comparison against independent Global Navigation Satellite Systems derived WTC at coastal stations show that the use of coastal WTC retrieval algorithms with modified inputs is able to significantly reduce the retrieval errors over these regions, with rms values of 3.1 cm between 5 and 10 km from the coast and 3.3 cm up to 5 km from the coast. For the Sentinel-3 MWR-derived operational WTC retrieval algorithm, these values are 9.2 cm between 5 and 10 km from the coast and 16.2 cm up to 5 km from the coast.**

***Index Terms*—Coastal regions, satellite altimetry, Sentinel-3, wet tropospheric correction (WTC).**

I. Introduction

THE wet tropospheric correction (WTC) is one of the major sources of uncertainty for the precise estimation of sea surface heights derived from satellite altimetry [1]. The corresponding path delay (PD) in the altimeter signal, which can reach almost 50 cm, is mostly due to the tropospheric water vapor content, and is characterized by a high spatial and temporal variability [2], [3]. Thus, for the purpose of retrieving the WTC, a nadir-looking microwave radiometer (MWR) is deployed in satellite altimetry missions, alongside the radar altimeter, whose observations allow for the most accurate way to retrieve this PD over open-ocean.

Two types of MWR are deployed on altimetric missions, with two or three frequency bands. The three-band MWR, best suited for the retrieval of the WTC, are deployed on the reference altimetric missions, namely TOPEX-Poseidon (T/P), Jason 1-3, and the most recent Sentinel-6 Michael Freilich. The two-band MWR operate on the complementary altimetry missions, namely ERS-1 and −2, Envisat, and Sentinel-3 missions from the European Space Agency (ESA), and on the Geosat Follow-On and SARAL/ALtiKa missions. The main frequency for both MWR types is located around the 22 GHz frequency, very close to the water absorption line peaked at the 22.235 GHz, mainly sensitive to the atmospheric water vapor content. The second frequency common to both MWR types is deployed in the 34–37 GHz window, particularly sensitive to the cloud liquid water content in the atmosphere. The third frequency, located around the 18 GHz, deployed only on MWR onboard the reference missions, allows for the consideration of sea surface effects. Additional high-frequency channels are being exploited for the first time on Sentinel-6, at 90, 130, and 168 GHz, with the experimental high-resolution microwave radiometer (HRMR), deployed alongside the advanced microwave radiometer for climate (AMR-C) for climate [4]. Data from the HRMR are expected to extend the WTC retrievals closer to the coast.

Over open-ocean, the relationship between the MWR brightness temperatures (TBs) and the WTC has been established by means of two main types of approaches. For the reference missions, a statistical log-linear algorithm has been used, function of the three-band TBs [5]. For the ESA Sentinel-3 mission, two types of MWR-derived WTC operational products are available, retrieved from neural network algorithms with three or five inputs, respectively, first developed for the Envisat mission [6], [7]. The three-inputs neural network (Op. 3I) considers the two MWR TBs, measured at 23.8 and 36.5 GHz, respectively, and the altimeter backscatter coefficient, σ_0, at Ku band. The five-inputs neural network (Op. 5I), an improvement of the first, considers additionally the sea surface temperature (SST), extracted from four static seasonal tables, and the atmospheric temperature lapse rate, γ_{800}, from a climatological table. Recent studies suggest the need for improvement of the Sentinel-3 MWR-derived WTC retrieval algorithms [8], [9].

Manuscript received 22 June 2023; revised 3 August 2023 and 11 August 2023; accepted 19 August 2023. Date of publication 25 August 2023; date of current version 7 September 2023. This work was supported by Fundação para a Ciência e a Tecnologia under Grant PRT/BD/153495/2021. *(Corresponding author: Pedro Aguiar.)*

The authors are with Departamento de Geociências, Ambiente e Ordenamento do Território, Faculdade de Ciências, Universidade do Porto, 4169-007 Porto, Portugal, and also with Centro Interdisciplinar de Investigação Marinha e Ambiental (CIIMAR), Terminal de Cruzeiros de Leixões, 4450-208 Matosinhos, Portugal (e-mail: pedro.aguiar@fc.up.pt; telmo.vieira@fc.up.pt; clazaro@fc.up.pt; mjfernan@fc.up.pt).

Digital Object Identifier 10.1109/JSTARS.2023.3308721

However, at coastal regions, the two main types of approaches described above between the MWR observations and the WTC fail. When approaching land, the mixed land/sea frequency-dependent footprints of the MWR result in increased anomalous values in the TBs observations due to land contamination. At the microwave region, between 18 and 34 GHz, land surfaces possess a higher and more variable emissivity than ocean surfaces. Moreover, since the MWR footprint sizes decreases with increasing frequency, this land contamination effect occurs at different stages of the approximation of the satellite to the coast, for each MWR frequency, with a first land contamination signature at the lowest frequency channel. As such, the operational WTC retrieval algorithms, trained over pure ocean conditions, compute PD corrections not accurate enough for coastal satellite altimetry applications. The MWR-derived WTC retrieval errors over coastal regions, predominantly due to the land contamination in the MWR observations, start to increase rapidly at distances from the coast in the range 20–30 km, depending on the altimetry mission [10].

Several approaches have been proposed in the literature with the purpose of minimizing the land contamination errors in the MWR observations [11], [12], [13]. In the approach proposed in [11], applied to special sensor microwave/imager (SSM/I) data observations, the problem of mixed land/sea footprints at coastal regions is addressed with the usage of a high-resolution land–sea mask to infer the fraction of water for each SSM/I observation. These corrected radiometer observations are then used in the open-ocean retrieval algorithm. The accuracy of the proposed data fusion technique is impacted by three main sources: 1) accuracy of the representation of the effective antenna pattern function (EAPF) of the SSM/I; 2) navigation uncertainty of the SSM/I; and 3) variations in the satellites' altitude, which leads to variations in the size of the EAPF of the SSM/I. The navigation uncertainty of the SSM/I was identified to be the dominant error source of the data fusion method.

In [12], several approaches are analyzed and two improved solutions, applied to T/P data measurements, are developed. The scarce ground-truth measurements available in coastal regions were identified as a major difficulty for the evaluation of the proposed methods. Nevertheless, of all the analyzed methods, the one proposed in [11] showed the best results.

In the studies mentioned above, the same approach is presented, which consists of the removal of the land contamination effects in the radiometer observations in such a way that the open-ocean retrieval algorithms can still be used over coastal regions. In [13], a different and more in-depth approach is presented, first designed for the Jason-2/OSTM advanced microwave radiometer (AMR). The method consists of the modification of the open-ocean log-linear WTC retrieval algorithm used for the reference missions, described in [5], to derive a new algorithm applicable over coastal regions, designed as Mixed-Pixel Algorithm (MPA). Instead of coefficients stratified by wind speed (WS) and a first PD approximation, the coefficients are now stratified by the land fraction (LF) in the frequency-dependent radiometer footprint and a first PD approximation. The modification of the stratification of the algorithm coefficients by WS to a stratification by LF is justified by the fact that the increase in the MWR TBs due to an increase in WS over open-ocean is undifferentiated from an increase in the formers due to an increase in the LF in the radiometer footprint over coastal regions. Moreover, the WS estimates used in the coefficient's stratification of the open-ocean log-linear algorithm are derived from MWR observations, and the former are also invalid in coastal regions. To account for the frequency-dependent radiometer footprint size, the LF parameter considered for the MPA coefficients stratification is the main beam LF of the lowest frequency channel. The MPA is valid up to an LF of 50% in the 18.7 GHz channel radiometer footprint.

Other approaches to compute the WTC in coastal regions using data from external sources were proposed [14], [15]. The Global Navigation Satellite Systems (GNSS) derived path delay plus (GPD+) algorithm, described in [14], combines data from several sources: GNSS stations in mainland coastal regions and islands; from satellite missions with scanning-imaging MWR, e.g., SSM/I; valid along-track MWR observations; and, ultimately, from European Centre for Medium-Range Weather Forecasts (ECMWF) atmospheric models. Through an objective analysis technique, the GPD+ algorithm estimates the WTC for altimeter observations with an invalid MWR-derived WTC, also possessing the ability to be applied to satellite altimetry missions without an onboard MWR.

In [15], the one-dimensional variational method is evaluated for the retrieval of the WTC in coastal areas. It combines a priori information on atmospheric and surface states, radiometer measurements, and additional information on emissivity and temperature to retrieve specific humidity and temperature profiles, which are then used to compute the WTC. The presence of clouds and rain have been identified to decrease the quality of the retrieval.

The methods described in [12] and [13] have been successfully applied to satellite altimetry missions with three-band MWR. No similar study has been found on the enhancement of the WTC in coastal regions focused on the usage of observations from missions with dual-band MWR, which lack the lower frequency channel.

Among the current altimeter missions, the Global Monitoring for Environment and Security Sentinel-3 mission from the Copernicus program is of particular interest and the focus of this study [16]. The Sentinel-3 mission is currently composed of two satellites: Sentinel-3A and Sentinel-3B. Each of the two satellites is composed of identical instruments, namely a dual frequency (Ku and C band) synthetic aperture radar altimeter (SRAL) and a dual-band passive MWR. Both satellites operate on the same near-polar, sun-synchronous orbit (orbit inclination of 98.65°), with a phase shift of $\pm 140°$ and a repeat cycle of 27 days each.

The aim of this study is to improve the WTC retrieval in coastal regions for the Sentinel-3 mission, based on modified improved TBs from the dual-band MWR, at 23.8 and 36.5 GHz, complemented with additional parameters to account for surface effects.

For this purpose, methods for improving the WTC retrieval parameters in coastal regions, TBs and σ_0, are proposed. These improved parameters are then used to estimate the WTC, first

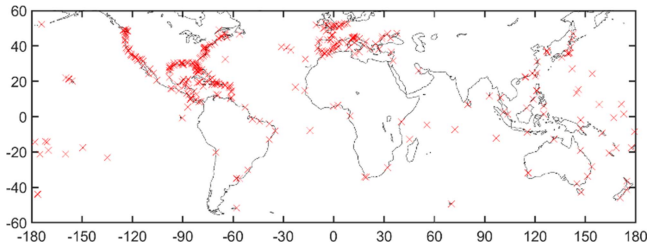

Fig. 1. GNSS stations location used for the independent assessment of the developed methodologies.

using an open-ocean algorithm and second using algorithms specifically trained over coastal regions, inspecting to what extent these new coastal algorithms outperform the open-ocean retrieval algorithms.

The article is organized as follows. A description of the data used, as well as the corresponding data processing steps, is provided in Section II. In Section III, the analysis, over coastal regions, of the WTC retrieval parameters is presented, and methods for their improvement are described. The development of coastal WTC retrieval algorithms is also described in Section III. In Section IV, a method for computing the LF in the MWR footprints aboard satellite altimeter missions, from external sources, is presented. In Section V, the results and discussion are outlined. Finally, in Section VI the conclusions are presented.

II. Data Description

Sentinel-3A Non-Time Critical (NTC) Level 2 ocean data products at 1 Hz (baseline collection 004), available from the European Organisation for the Exploitation of Meteorological Satellites (EUMETSAT) Data Store, were processed over coastal regions. Valid measurements with no rain or ice contamination, within the $[-50°, 50°]$ latitude range, and with a distance from the nearest coast between 0 and 60 km were considered.

Two datasets were developed, each composed of 2 years of Sentinel-3A SRAL and MWR measurements. The first dataset, with measurements from Sentinel-3A cycles 12 to 38, was used for the development of the methodologies (development dataset). The second dataset comprises measurements from Sentinel-3A cycles 39 to 66 (test dataset). The latter was used for the independent assessment of the developed methodologies, using a noncollocated comparison against zenith wet delays (ZWD) from inland coastal and islands GNSS stations, and against the WTC derived from the ECMWF ERA5 atmospheric model [17]. The processing of the GNSS stations data is described below.

GNSS stations from three GNSS networks, the International GNSS Service (IGS), SuomiNet, and EUREF Permanent GNSS Network(EPN), were selected based on a maximum distance to the nearest coast of 100 km and a maximum orthometric height of 100 m. The last filtering condition aims to mitigate the errors derived from the height reduction method of the WTC, further explained below. A total of 381 GNSS stations match these filtering conditions. In Fig. 1, the location of the GNSS stations used for the assessment is illustrated.

For each GNSS station, zenith total delay (ZTD) measurements, with a time-step of 30–60 min are available. These can be expressed as the sum of the wet and hydrostatic components (ZWD and ZHD, respectively). Thus, the ZWD can be expressed as

$$\mathrm{ZWD} = \mathrm{ZTD} - \mathrm{ZHD}. \tag{1}$$

The ZHD component used in (1) was computed from sea level pressure (SLP) grids from the ECMWF ERA5 model, with 0.25° by 0.25° spatial resolution and available every 6 h, in two steps. First, the total atmospheric pressure, P_s, at the orthometric height of each GNSS station, H_s, was computed from ERA5 SLP values, according to [18]. Second, the ZHD was computed from P_s using the modified Saastamoinen model, first described in [19] and later modified by [20].

The ZWD component obtained from (1) is referred to each station orthometric height. Thus, a height reduction to sea level needs to be applied. For this purpose, the Kouba reduction method, described in [21], was adopted, which can be used up to height reductions of 1000 m. Therefore, the threshold in the GNSS stations orthometric height (100 m) was set to mitigate errors coming from the Kouba reduction method.

The colocation method between Sentinel-3A SRAL/MWR observations and GNSS stations was conducted individually for each GNSS station. In a first step, for each station location, all the Sentinel-3A SRAL/MWR observations with a maximum distance of 80 km were considered. Second, a time colocation method was applied individually for each altimeter observation. A linear time interpolation method was applied to derive the GNSS ZWD observation for each altimeter measurement, considering the GNSS observations, in time, immediately before and after the altimeter observation. A maximum absolute time difference of 30 min was considered between the altimeter observation and the two used GNSS observations mentioned earlier.

For the ECMWF ERA5 model, the reference WTC values were computed from atmospheric temperature, T, and specific humidity, q, grids at pressure levels, with 0.25° by 0.25° spatial resolution and available every 3 h, obtained from the Copernicus Climate Change Service (C3S) Climate Data Store (CDS) [22]. The WTC was computed through a numerical integration method of q and T at 37 pressure levels, from 1000 to 1 hPa, and space–time interpolated to each Sentinel-3A SRAL measurement position. The numerical integration method provides the most accurate way to compute the WTC from atmospheric models. More details on the mathematical formulation can be found in [2].

III. Improvement Over Coastal Regions of the Sentinel-3A WTC Retrieval Parameters and Algorithms

The need for improvement of the two Sentinel-3 MWR-derived WTC operational products has already been addressed [8], [9]. In [8], a new learning dataset for the Sentinel-3 mission was developed for open-ocean. Several algorithms were developed, focused on the combination of different inputs.

Results showed that the consideration of a dynamic SST, i.e., space–time interpolated for each altimeter position, from the ECMWF ERA5 atmospheric model, improves the WTC retrieval. Moreover, the use of a dynamic atmospheric temperature lapse rate, γ_{800}, alongside the dynamic SST, provided redundant information.

In this section, an analysis of the WTC retrieval parameters over coastal regions is presented. In order to remove the land contamination effects, methods of modification of the two Sentinel-3A MWR TBs are presented. These modified TBs are then used alongside the Sentinel-3A SRAL σ_0 parameter, at Ku band, in the three-inputs open-ocean UP3S0 algorithm described in [8] to retrieve the WTC.

A modification method of the SRAL σ_0 is also presented. In this context, an additional goal is to explore to what extent the usage of WS from the ECMWF ERA5 atmospheric model, instead of the observed or modified SRAL σ_0 measurements, enhances the WTC retrieval over coastal regions. For this last approach, the open-ocean UP3WS algorithm described in [8] is also exploited. This algorithm considers as inputs the two Sentinel-3A MWR TBs alongside the 10-m U and V components of WS from the ECMWF ERA5 model.

At last, a description of the development of WTC retrieval algorithms specifically trained over coastal regions is provided. The aim is to explore to what extent these new coastal algorithms outperform the open-ocean retrieval algorithms.

A. Analysis of the Sentinel-3A WTC Retrieval Parameters Over Coastal Regions

Aiming at characterizing, over coastal regions, the various parameters used in the WTC retrievals, a first task was to analyze the Sentinel-3A SRAL and MWR parameters of interest in these regions. In Fig. 2, the mean and standard deviation of the Sentinel-3A MWR 23.8 and 36.5 GHz TBs and the SRAL backscatter coefficient σ_0, at Ku band, are illustrated, computed in classes of 5 km width from distance to the nearest coast, using data from the Sentinel-3A development dataset.

In the range of 20–60 km from the coast, a stable value of the two MWR TBs is observed, both in terms of the mean and the standard deviation, with higher values for the 23.8 GHz channel. An exponential increase of the mean value is observed for both MWR channels, starting from about 20 km from the coast. It can also be observed that this exponential increase starts slightly closer to the coast for the 36.5 GHz channel, which is in line of agreement with its smaller footprint size relative to the 23.8 GHz channel footprint size. In terms of the standard deviation, an exponential increase is observed for the 36.5 GHz channel starting at 10 km from the coast.

An almost linear increase is observed for the Sentinel-3A SRAL σ_0 for decreasing distance from the coast, in the range of distance from the coast between 20 and 60 km, both in terms of the mean and the standard deviation. From 20 km and up to the coast, this linear increase in both statistical parameters changes to an almost exponential increase.

In Fig. 3, the same analysis presented in Fig. 2 is depicted for the two Sentinel-3A radiometer WTC operational products (Op. 3I and Op. 5I, respectively), as well as for the WTC derived from the ECMWF Operational Model (ECMWF Op.) [23] (available in the Sentinel-3A products, alongside the Op. 3I and Op. 5I radiometer WTC). The mean and standard deviation values are presented in terms of the Wet Path Delay (WPD $= -$WTC).

In terms of the mean of the WPD, an exponential increase is observed for the WPD derived from both radiometer geophysical retrieval algorithms (Op. 3I and Op. 5I, respectively), starting from about 25 km from the coast. This increase is very similar to those observed for the MWR TBs in Fig. 2, which can be explained by the high relative importance between the TBs and the WPD. In terms of the mean value, the WPD derived from the ECMWF Op. does not show this increase due to land

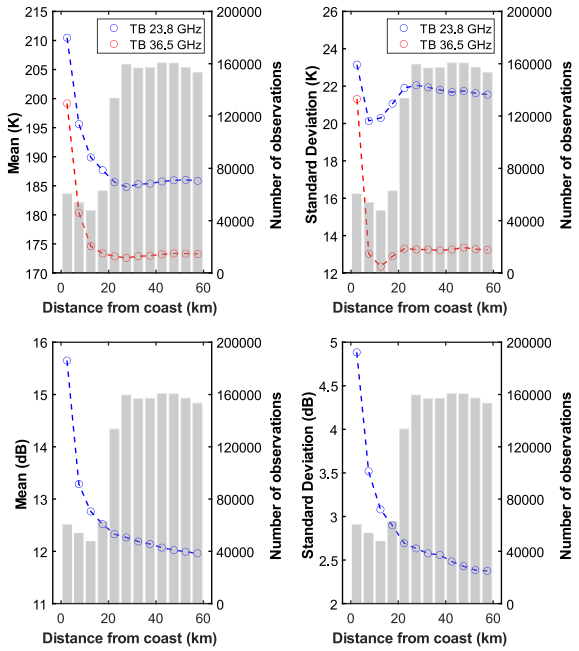

Fig. 2. Mean (left) and standard deviation (right) of the Sentinel-3A MWR 23.8 (blue) and 36.5 GHz (red) brightness temperatures (top) and the SRAL backscatter coefficient σ_0, at Ku band (bottom), computed in classes of 5 km width from distance to the nearest coast using data from the Sentinel-3A development dataset. Grey bars represent the number of observations available in each class.

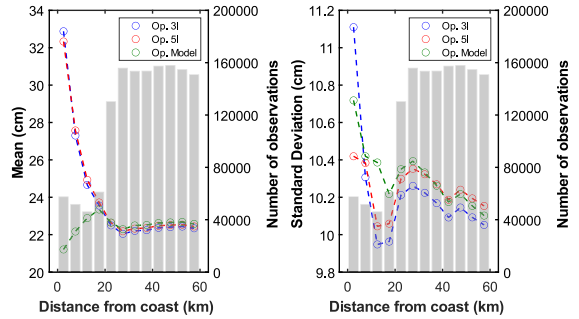

Fig. 3. Mean (left) and standard deviation (right) of the two Sentinel-3A radiometer wet path delay operational products (Op. 3I and Op. 5I, respectively), and the wet path delay derived from the ECMWF operational model, computed in classes of 5 km width from distance to the nearest coast using data from the Sentinel-3A development dataset. Grey bars represent the number of observations available in each class.

contamination. The increased variability observed for the three WPD analyzed products is not significantly impactful, with a maximum increase of the standard deviation of approximately 1 cm for the Op. 3I WPD.

B. Modification of the Sentinel-3A MWR Brightness Temperatures

As shown in the last subsection, and stated in previous articles, the land contamination in the MWR TBs is the predominant error source for the accurate retrieval of the WTC in coastal regions. As such, previous articles have focused on the removal of the land contamination effects in such a way that the open-ocean retrieval algorithms are still applicable.

In this subsection, a proposal for the modification of the Sentinel-3A MWR TBs is presented, in order to mitigate land contamination effects. The method consists of the application, for each measurement, of the following correction:

$$\text{Corr} = \langle \text{TB}(f) \rangle_{(d,\ \text{WPD})} - \langle \text{TB}(f)_{\text{ocean}} \rangle_{\text{WPD}} \qquad (2)$$

where $\langle \text{TB}(f) \rangle_{(d,\ \text{WPD})}$ is the mean value of the Sentinel-3A MWR TBs, for each frequency, parametrized by classes of distance from coast, d, with 5 km width between 0 and 25 km, and WPD classes from the ECMWF Op., with 5 cm width between 0 and 50 cm. $\langle \text{TB}(f)_{\text{ocean}} \rangle_{\text{WPD}}$ is the mean value over open-ocean, computed using the observations in the range 25–60 km of distance from the coast and parametrized by WPD classes, as described. Thus, for each Sentinel-3A MWR TB observation, the applied modification is function of the satellite distance from coast and of a first WPD value, and consists of the subtraction, for each MWR frequency, of the excess in TBs relative to the mean open-ocean TBs values. The closer to the coast and greater the first WPD value from the ECMWF Op., the greater the applied modification. The parametrization by WPD classes aims to account for the temporal and spatial variability of the TB observations, which are related to the corresponding space–time variability of the atmospheric water vapor.

A second approach, more in line with the methods described in [13], consists of switching the parametrization by classes of distance from coast, outlined in (2), to classes of LF in the radiometer footprint, depending on the frequency. This method is expected to present a better performance than the previous, since the parametrization by classes of distance from coast can be misleading. For instance, in the cases where the satellite is close to islands, the distance to the nearest coast is small, although the land contamination can be also small, depending on the island size. Thus, decreasing distances from the coast are not necessarily related to increasing LF values for each radiometer channel footprint. The new correction method takes the form

$$\text{Corr} = \langle \text{TB}(f) \rangle_{(\text{LF},\ \text{WPD})} - \langle \text{TB}(f)_{\text{ocean}} \rangle_{\text{WPD}} \qquad (3)$$

where $\langle \text{TB}(f) \rangle_{(\text{LF},\ \text{WPD})}$ is the mean value of the Sentinel-3A MWR TBs, for each frequency, parametrized by classes of LF in the frequency-dependent MWR footprint, with 0.05 width between 0 and 1 (0 corresponds to pure ocean scenes and 1 to MWR footprints completely over land), and WPD classes from the ECMWF Op., with 5 cm width between 0 and 50 cm. For this second approach, the mean value over open-ocean, $\langle \text{TB}(f)_{\text{ocean}} \rangle_{\text{WPD}}$, is computed using the MWR observations for which the LF is equal to zero (LF = 0) and parametrized by WPD classes as described earlier.

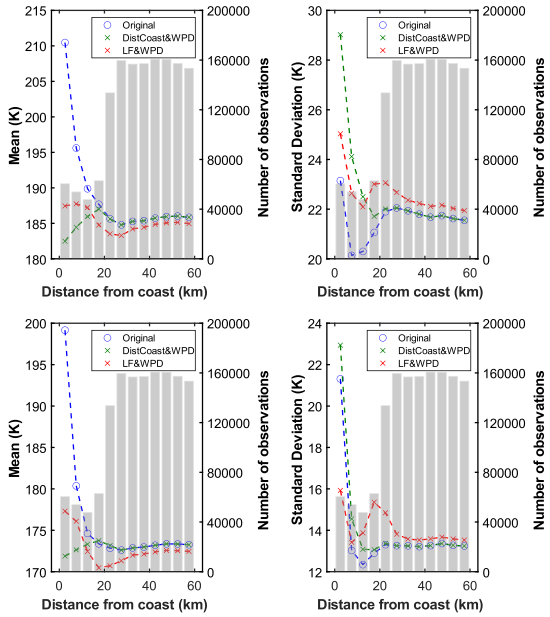

Fig. 4. Mean (left) and standard deviation (right) of the Sentinel-3A MWR 23.8 and 36.5 GHz brightness temperatures (top and bottom panels, respectively), alongside the same brightness temperatures values obtained from the application of the two modification methods (DistCoast&WPD and LF&WPD, respectively). Computed in classes of 5 km width from distance to the nearest coast using data from the Sentinel-3A development dataset. Grey bars represent the number of observations available in each class.

Hence, the modification of the Sentinel-3A MWR TBs is now function of the LF in the frequency-dependent MWR footprint, and a first WPD value from the ECMWF Op. The method works in the same way as described before, and the applied modification is greater the greater the LF and the first WPD values.

Unlike the reference altimetry missions, such as Jason-3 and Sentinel-6, for the Sentinel-3 mission, the LF values for the two MWR frequency channels are not provided in the Level-2 NTC products. Thus, for this purpose, a method to compute the LF values, for each Sentinel-3A MWR frequency channel, relying on the Global Surface Water (GSW) Dataset [24], has been applied. This method is described in detail in Section IV. It possesses the ability to be applied to any satellite altimetry mission with an onboard MWR, given that the respective frequency-dependent footprint sizes are known. For the Sentinel-3A satellite, the MWR footprint sizes are 22.93 and 18.29 km for the 23.8 and 36.5 GHz frequencies, respectively [9].

In Fig. 4, similar to Fig. 2, the mean and standard deviation of the Sentinel-3A MWR 23.8 and 36.5 GHz TBs are illustrated, alongside the same TB values obtained from the application of the two modification methods described earlier, computed in classes of 5 km width from distance to the nearest coast, using data from the Sentinel-3A development dataset. Both methods of modification of the TBs are able to significantly reduce the

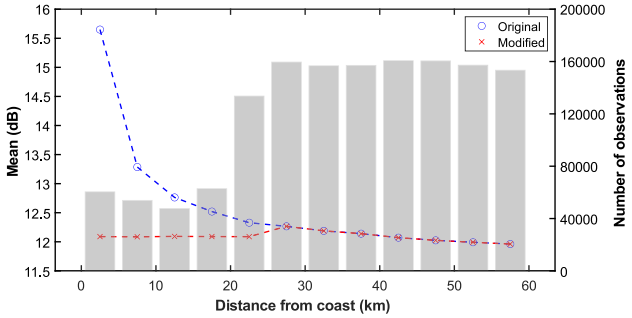

Fig. 5. Mean of the Sentinel-3A SRAL backscatter coefficient σ_0, at Ku band, alongside the modified σ_0 parameter, computed in classes of 5 km width from distance from the nearest coast using data from the Sentinel-3A development dataset. Grey bars represent the number of observations available in each class.

respective land contamination effects for both MWR frequency channels.

C. Modification of the Sentinel-3A SRAL Backscatter Coefficient σ_0

Similar to the MWR TBs, the Sentinel-3A SRAL σ_0 parameter, at Ku band, shows an almost exponential increase over coastal regions, as depicted in Fig. 2. Thus, since this parameter is used alongside the MWR TBs to compute the WTC for the Sentinel-3 mission, a proposal of modification of the Sentinel-3A SRAL σ_0, similar to the methods of modification described in the last subsection for the MWR TBs, is presented in this subsection. The correction method, applied for each SRAL σ_0 measurement, is of the form

$$\text{Corr} = \langle \sigma_0 \rangle_d - \langle \sigma_{0\ \text{ocean}} \rangle \tag{4}$$

where $\langle \sigma_0 \rangle_d$ is the mean value of the Sentinel-3A SRAL σ_0, parametrized by classes of distance from coast, d, with 5 km width between 0 and 25 km, and $\langle \sigma_{0\ \text{ocean}} \rangle$ is the mean value over open-ocean, computed using the observations in the range 25–60 km of distance from the coast. Thus, for each Sentinel-3A SRAL σ_0 observation, the modification method is only function of the satellite distance from coast. As in the cases outlined before, it consists of the subtraction of the excess in σ_0 relative to the mean open-ocean values, with increasing modifications for decreasing distance from the coast.

In the case of the SRAL σ_0, the development of the correction method parametrized by classes of distance from coast, instead of MWR LF classes, is due to the lower relative importance of σ_0 with the WTC, when compared to the MWR TBs weight. Thus, a simpler correction method can be adopted.

In Fig. 5, the mean value of the Sentinel-3A SRAL σ_0, at Ku band, is presented, alongside the same parameter obtained after applying the modification method described earlier, computed in classes of 5 km width from distance to the nearest coast, using data from the Sentinel-3A development dataset. Quantitively, the modification method is able to significantly reduce the σ_0 parameter over coastal regions. Given the mathematical formulation of the modification method, the standard deviation values are the same as the ones for σ_0 with no modifications applied, which are already presented in Fig. 2.

TABLE I
ALGORITHM DESCRIPTION FOR THE FOUR DEVELOPED COASTAL ALGORITHMS

Algorithm	Algorithm Description
C2C UP1	Unmodified MWR TBs and unmodified SRAL σ_0
C2C UP2	Modified MWR TBs and modified SRAL σ_0
C2C UP3	Modified MWR TBs, modified SRAL σ_0 and SST from the ERA5 model
C2C UP4	Modified MWR TBs, modified SRAL σ_0 and SST, and γ_{800} from the ERA5 model

D. Development of the Coastal Wet Tropospheric Correction Retrieval Algorithms

For the purpose of the development of WTC retrieval algorithms specifically trained in coastal regions, a random split of train and validation measurements was applied to the Sentinel-3A development dataset, described in Section II. Only observations in the range 0–20 km of distance from the nearest coast were considered for this train/validation split, in order to strictly limit the learning of the algorithms to land contamination scenes. From all the observations from the Sentinel-3A development dataset within this range of distance from coast, 80% compose the train database (179 961 measurements) and 20% (44 990 measurements) refer to the validation database.

A total of four neural network algorithms were developed. All algorithms were trained with the stochastic gradient descent with momentum retro-propagation algorithm, and all consider the same architecture used for the operational WTC retrieval algorithms of the Sentinel-3 mission: neural networks with one hidden layer with eight neurons and the tan-sigmoid activation function, with a linear output regression layer [6], [7]. Thus, the difference between all algorithms relies on the number and type of inputs used, as described below. A brief description of each developed coastal algorithm is presented in Table I.

The first coastal neural network algorithm (denoted C2C UP1) considers the two Sentinel-3A MWR TBs, at 23.8 and 36.5 GHz, and the SRAL σ_0, at Ku band, with no modifications applied to either of the inputs.

The second algorithm (denoted C2C UP2) considers the same three inputs of the first algorithm, with modifications applied to both the MWR TBs and the SRAL σ_0 from the methods described in the previous subsections.

The third algorithm (denoted C2C UP3) is the same as C2C UP2, with the addition of the SST from the ECMWF ERA5 model, space–time interpolated to each Sentinel-3A SRAL position. Relative to the third algorithm, the fourth algorithm (denoted C2C UP4) also considers the atmospheric temperature decrease rate, γ_{800}, from the ECMWF ERA5 model.

The validation database purpose is to evaluate the quality of the training process for each developed algorithm. As output, each algorithm returns the WPD, in cm. The SST input used in the last two coastal algorithms is the SST_{skin}, defined as the temperature of the ocean up to a maximum depth of $\sim$10 μm. ECMWF ERA5 atmospheric model grids with a 0.50° by 0.50° spatial resolution and available every 6 h, obtained from the

C3S CDS [25], were used. For the fourth coastal algorithm, γ_{800} global grids with 0.25° by 0.25° spatial resolution and available every 3 h were adopted. These grids were created from ECMWF ERA5 atmospheric temperature grids at pressure levels, obtained from the C3S CDS [22]. Each γ_{800} value results from the application of a linear fit to the atmospheric temperature using the ERA5 pressure levels between 1000 and 800 hPa.

The reference WPD values used in the development of the coastal algorithms were derived from the ECMWF ERA5 atmospheric model, computed from the numerical integration method of specific humidity and atmospheric temperature described in Section II.

IV. Computation of MWR Land Fractions From the Global Surface Water Dataset for Satellite Altimetry Missions

The GSW Dataset provides information on the spatial and temporal distribution of surface water globally over the last 38 years, with 30-m spatial resolution. Details on the development of this database can be found in [24]. Different types of information are provided, namely the water occurrence, which shows where surface water occurred over the 38 years period. Permanent water surfaces have 100% occurrence, whereas permanent land surfaces have 0% occurrence.

The GSW occurrence dataset is provided globally in a total of 504 tiles of 10° by 10° each, with 0.00025° resolution (40 000 by 40 000 pixels). This level of detail makes its routine use impracticable; therefore, a first task was to resample the dataset to a lower resolution. The resample process consisted of the computation of the mean occurrence value in a 64 by 64 pixels sliding window, with a final spatial resolution of 0.016° (∼1.78 km, at the equator).

The GSW occurrence possesses a complementary relationship with LF. Therefore, one can easily compute $\mathrm{LF_{GSW}}$ for each GSW grid pixel from the occurrence values ($\mathrm{Occ_{GSW}}$), with the following equation:

$$\mathrm{LF_{GSW}} = \frac{100 - \mathrm{Occ_{GSW}}}{100}. \tag{5}$$

To compute the LF values for each MWR channel, for satellite altimetry missions possessing an onboard MWR, one has to account for the respective frequency-dependent footprint size. The developed method from the GSW Dataset can be applied to any satellite altimetry mission with an onboard MWR. First, the GSW grid values within a predefined search radius, in degrees, centered in the MWR measurement position and function of the respective footprint size on the ground, are determined. Additionally, this search radius is weighted by the convergence of the meridians for increasing latitudes. Second, the mean $\mathrm{LF_{GSW}}$ is computed from this subset of values within the MWR footprint.

Since the Jason-3 products provide the main beam LF for each AMR frequency channel, the method was first applied to the Jason-3 AMR, followed by the assessment of the computed $\mathrm{LF_{GSW}}$ against the ones provided in the products. In this way, the performance of the method could be evaluated prior to its application to the Sentinel-3 mission.

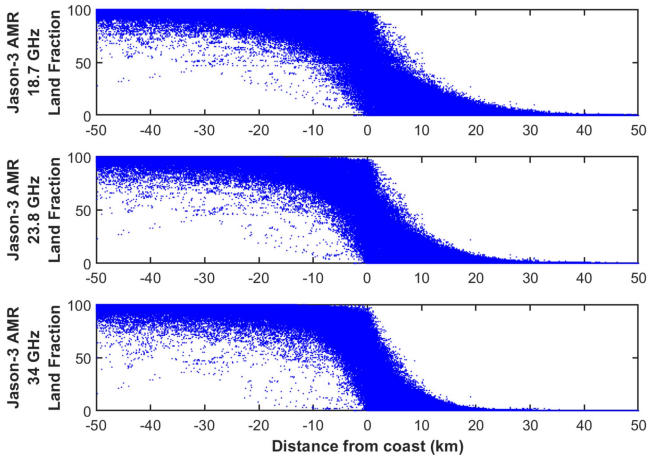

Fig. 6. Scatter plots of the main beam land fractions for the 18.7, 23.8, and 34 GHz channels of the Jason-3 AMR, evaluated against the corresponding distance from the nearest coast. Measurements over land possess a negative distance from coast.

Jason-3 GDR-F, Level-2 NTC data products, available from AVISO+, were processed over coastal regions. Observations from cycles 34, 43, 52, and 61 were filtered by latitudes in the range [−50°, 50°] and within the range [−50, 50] km of distance from the nearest coast (measurements over land possess negative distance to the coast). For these range of distance to the coast, AMR footprints completely over land and completely over sea, as well as mixed land/sea footprints, are available and the method can be evaluated for these three footprint conditions.

In Fig. 6, the main beam LF for the 18.7, 23.8, and 34 GHz channels of the Jason-3 AMR are evaluated against the corresponding distances from the nearest coast.

A clear increase of the LF values is observed with the approximation of the satellite to the coast. As expected, this increase starts at different distances from coast for the three AMR frequencies. Very close to the coast, a wide spread of LF values is observed for the whole range of main beam LF, sustaining the beforementioned idea, in subsection *B* of the last section, that decreasing distances from the coast are not strictly related to increasing LF values for each radiometer channel footprint.

For each Jason-3 measurement, the LF computation method from the GSW Dataset described above was applied. The footprint sizes for the 18.7, 23.8, and 34 GHz were defined as 41.6, 36.1, and 22.9 km, respectively, as described in [26]. For each AMR frequency, an assessment has been performed against the main beam LF values provided in the Jason-3 Level-2 NTC products. The mean, standard deviation, and root mean square (rms) values of the differences $\mathrm{LF_{AMR}} - \mathrm{LF_{GSW}}$ (in percentage) were evaluated individually for the three possible LF scenes: pure ocean scenes, where $\mathrm{LF_{AMR}} = 0\%$; mixed sea/land scenes, where $\mathrm{LF_{AMR}} \in]0, 100[\ \%$; and pure land scenes, where $\mathrm{LF_{AMR}} = 100\%$. The results are summarized in Table II.

A negative mean difference between $\mathrm{LF_{AMR}}$ and $\mathrm{LF_{GSW}}$ is observed for all three AMR frequencies, both for pure ocean and mixed sea/land scenes, indicating an overestimation of the LF values computed from the GSW Dataset relative to the ones provided for each AMR channel. The statistics of the differences

TABLE II
MEAN, STANDARD DEVIATION, AND RMS OF THE DIFFERENCES $LF_{AMR} - LF_{GSW}$ (IN PERCENTAGE), FOR EACH JASON-3 AMR FREQUENCY CHANNEL

Jason-3 AMR frequency	Mean (%)	Standard deviation (%)	RMS (%)
Pure ocean scenes ($LF_{AMR} = 0\%$)			
18.7 GHz	–2.7	10.4	10.7
23.8 GHz	–2.2	9.7	10.0
34 GHz	–1.9	9.8	10.0
Mixed sea/land scenes ($LF_{AMR} \in]0, 100[\%$			
18.7 GHz	–3.4	6.7	7.5
23.8 GHz	–3.6	6.7	7.6
34 GHz	–4.1	8.1	9.0
Pure Land scenes ($LF_{AMR} = 100\%$)			
18.7 GHz	0.1	0.4	0.4
23.8 GHz	0.1	0.6	0.6
34 GHz	0.1	0.7	0.7

for pure land scenes are very satisfactory, with values inferior to 1%. Nevertheless, the most crucial results to analyze are the ones for mixed sea/land scenes, since coastal regions are characterized by this type of radiometer footprint scenes. For the MPA, described in [13] and first developed for the Jason-2 AMR, a 10% relative error was assumed for the 18.7 GHz LF. For this purpose, a maximum error tolerance of 10% was also defined, and the results of the rms of the differences are satisfactory given this tolerance. Nevertheless, just as in the case of the MPA, a 10% maximum error is conservative since the computed LF values are only used for choosing the parameters for the MWR TBs modification method, presented in Section III-B, which are binned by LF and WPD classes.

V. RESULTS AND DISCUSSION

A. Independent Assessment Against Inland Coastal and Islands GNSS Stations

A total of 116 416 measurements from Sentinel-3A SRAL/MWR cycles 39 to 66 (test dataset) were successfully collocated, in time and space, with inland coastal and islands GNSS stations. Since the colocation methods were performed individually for each GNSS station, the same Sentinel-3A SRAL/MWR measurement can have a successful colocation with more than one GNSS station. Thus, for these cases, the colocation for which the distance to the GNSS station is minimum was kept, and the others discarded. The new dataset used for the independent assessment with GNSS stations is composed of 95 799 Sentinel-3A SRAL/MWR measurements.

In a first phase, the evaluation of the two methods of modification of the Sentinel-3A MWR TBs (function of classes of distance from coast and function of MWR LF) was conducted. For this purpose, the modified TBs were used alongside the Sentinel-3A SRAL σ_0, at Ku band, in the open-ocean UP3S0 algorithm, described in [8], to derive the WTC. The first algorithm, denoted O2C UP3S01, considers the MWR TBs modified by distance from coast and WPD classes, whereas the second algorithm, denoted O2C UP3S02, considers the MWR TBs

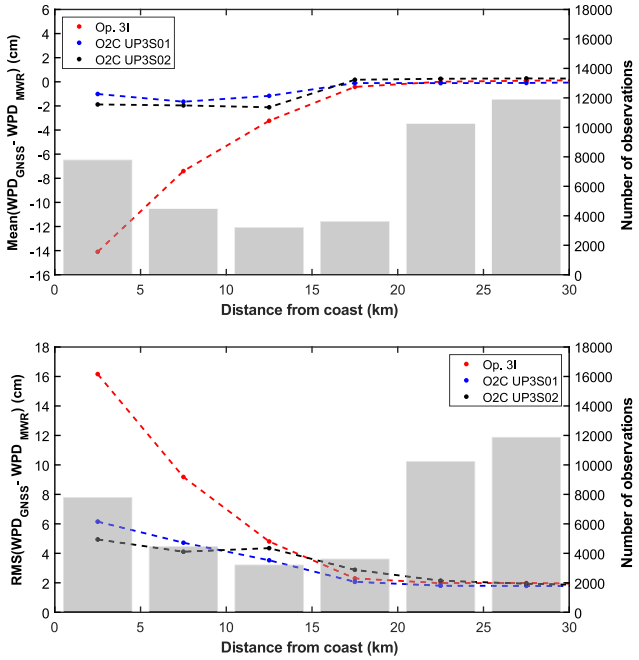

Fig. 7. Mean (top) and rms (bottom) of the differences $WPD_{GNSS} - WPD_{MWR}$, in classes of 5 km width of distance from coast, for the Sentinel-3A three-inputs MWR operational algorithm (Op. 3I), and the UP3S0 algorithm with TBs modified by distance from coast and WPD classes (O2C UP3S01) and modified by MWR land fraction and WPD classes (O2C UP3S02). Grey bars represent the number of observations.

modified by MWR LF and WPD classes. The mean and rms of the differences $WPD_{GNSS} - WPD_{MWR}$ are presented in Fig. 7, in classes of 5 km width of distance from coast.

In terms of the mean of WPD differences, a clear exponential decrease is observed for the Sentinel-3A MWR Op. 3I algorithm as approaching the coast, which can reach −14 cm for the first class of distance from coast. This behavior may be explained by the optimization of the algorithm toward open-ocean conditions. Over open-ocean, high values of the MWR TBs are associated to high WPD values. However, over coastal regions, the land contamination effects results in increased TBs, as already seen in Fig. 2. As such, the algorithm computes high WPD values since this is the relationship "learned" over open-ocean. When compared to GNSS observations, the radiometer WPD values are overestimated relative to the first, with a decrease in the mean of the differences $WPD_{GNSS} - WPD_{MWR}$ up to the coast in line with the land contamination effects.

This behavior is not observed for the two WPD corrections computed from the UP3S0 algorithm with modified TBs (O2C UP3S01 and O2C UP3S02, respectively). The two proposed approaches of modification are able to significantly reduce the mean and rms of WPD differences, with an improvement in the rms, relative to the Sentinel-3A MWR Op. 3I algorithm, in the order of 10 cm up to 5 km of distance from coast. For the O2C UP3S01 algorithm, the rms of WPD differences is 4.7 cm between 5 and 10 km from coast and 6.2 cm up to 5 km from coast. The O2C UP3S02 algorithm rms values are 4.1 cm between 5 and 10 km from coast and 4.9 cm up to 5 km from coast. Thus, for the first two classes of distance from coast, the

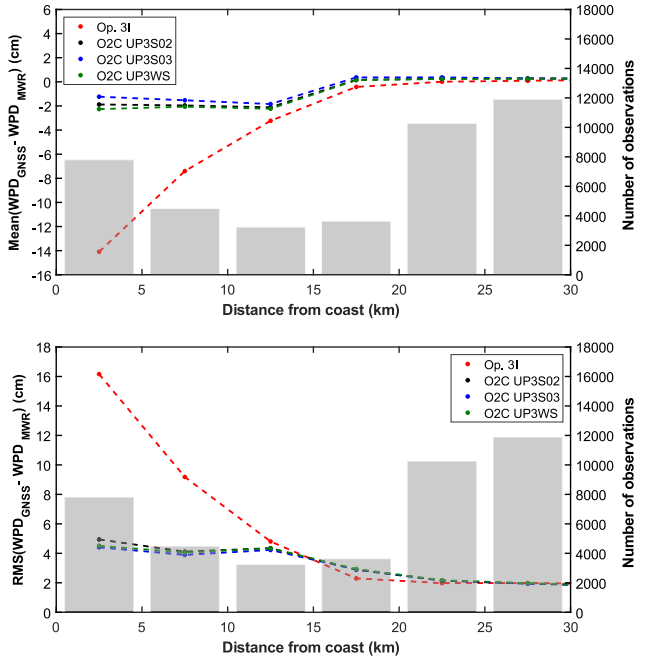

Fig. 8. Mean (top) and rms (bottom) of the differences $\mathrm{WPD_{GNSS}} - \mathrm{WPD_{MWR}}$, in classes of 5 km width of distance from coast, for the Sentinel-3A three-inputs MWR operational algorithm (Op. 3I), the UP3S0 algorithm with modified TBs (O2C UP3S02) and a modified σ_0 (O2C UP3S03), and the UP3WS algorithm with modified TBs and the 10-m U and V wind-speed components of the ERA5 model (O2C UP3WS). Grey bars represent the number of observations available in each class.

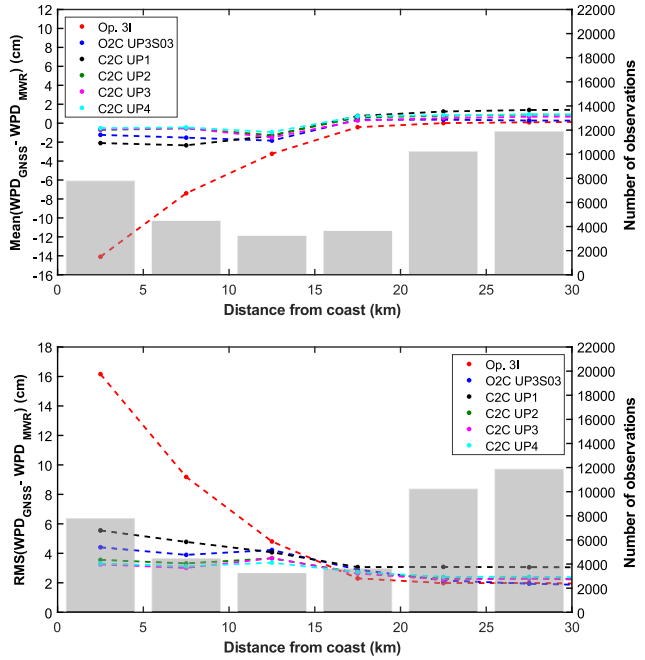

Fig. 9. Mean (top) and rms (bottom) of the differences $\mathrm{WPD_{GNSS}} - \mathrm{WPD_{MWR}}$, in classes of 5 km width of distance from coast, for the Sentinel-3A three-inputs MWR operational algorithm (Op. 3I), the UP3S0 algorithm with modified TBs and a modified σ_0 (O2C UP3S03), and the four developed coastal algorithms. Grey bars represent the number of observations available in each class.

approach of modification of the TBs parametrized by classes of MWR LF and a first WPD value (O2C UP3S02) shows a better performance than the first TBs modification approach (O2C UP3S01).

On a second phase, the modification method for the Sentinel-3A SRAL σ_0, parametrized by classes of distance from coast, was evaluated. In parallel, the substitution of σ_0 by the 10-m U and V components of WS, from the ECMWF ERA5 model, was also evaluated. The modified σ_0 was used alongside the modified MWR TBs, using the methods of modification by MWR LF and a first WPD value from the ECMWF Op., in the UP3S0 algorithm (O2C UP3S03 algorithm). For the second approach, the 10-m U and V components of WS from the ECMWF ERA5 model were used in the UP3WS algorithm, also described in [8], alongside the same modified MWR TBs (O2C UP3WS algorithm). The results are presented in Fig. 8.

The use of a modified SRAL σ_0 (O2C UP3S03), instead of the one with no modifications applied (O2C UP3S02), further improves the WTC retrieval in coastal regions. However, the improvement is significantly lower relative to the improvements observed in Fig. 7, given the lower relative importance of σ_0 against the MWR TBs for the WTC retrieval. The corresponding rms of WPD differences for the O2C UP3S03 algorithm is 3.9 cm between 5 and 10 km from the coast and 4.4 cm up to 5 km from the coast. Thus, relative to the O2C UP3S02 algorithm, rms reductions of 0.2 cm between 5 and 10 km from the coast and 0.5 cm up to 5 km from the coast have been achieved.

The use of the 10-m U and V components of WS from the ECMWF ERA5 model (O2C UP3WS), instead of the SRAL σ_0 input with no modifications applied (O2C UP3S02), also improves the retrieval, although the results of the rms of WPD differences are in line of agreement with the ones with the modified SRAL σ_0 input (O2C UP3S03), with rms values of 4.1 cm between 5 and 10 km from the coast and 4.5 cm up to 5 km from the coast.

The third and last step was the assessment of the four developed coastal WTC retrieval algorithms. The first coastal algorithm (C2C UP1) considers the two Sentinel-3A MWR TBs and the SRAL σ_0 with no modifications applied to either of the inputs. Given the results presented in Figs. 7 and 8, all the remaining three algorithms (C2C UP2, C2C UP3, and C2C UP4) take as input the MWR TBs modified by classes of MWR LF and a first WPD value from the ECMWF Op., and the SRAL σ_0 modified by classes of distance from coast. Additionally, the C2C UP3 algorithm considers the $\mathrm{SST_{skin}}$ input and the C2C UP4 algorithm the $\mathrm{SST_{skin}}$ and γ_{800} inputs, from the ECMWF ERA5 model. The results are presented in Fig. 9.

A clear improvement is observed with the usage of coastal algorithms with modified MWR TBs and modified SRAL σ_0 inputs, relative to the open-ocean UP3S0 algorithm with the same three modified inputs (O2C UP3S03). In fact, with the exception of the C2C UP1 algorithm, all the remaining developed coastal algorithms show a mean of WPD differences of 1 cm or lower, in absolute value, in the first 10 km from coast. The inclusion of the $\mathrm{SST_{skin}}$ input from the ECMWF ERA5 model in C2C UP3 algorithm further improved the results of the rms of WPD

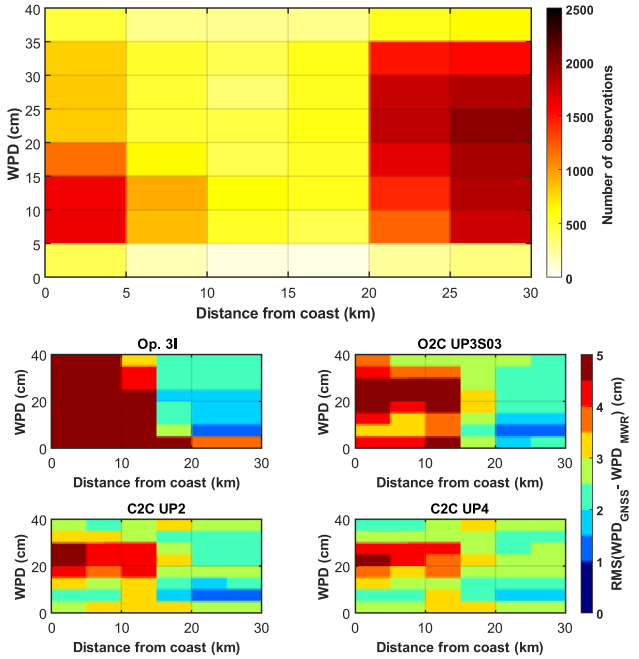

Fig. 10. RMS of the differences $\mathrm{WPD_{GNSS}} - \mathrm{WPD_{MWR}}$, in classes of 5 km width of distance from coast and classes of 5 cm width of a first WPD value from the ECMWF operational model, for the Sentinel-3A three-inputs MWR operational algorithm (Op. 3I), the open-ocean UP3S0 algorithm with modified TBs and a modified σ_0 (O2C UP3S03), and the second and fourth developed coastal algorithms (C2C UP2 and C2C UP4, respectively). The top figure shows the number of observations for each image tile.

differences, relative to the results for C2C UP2 algorithm, with rms values of 3.0 cm between 5 and 10 km from the coast and 3.3 cm up to 5 km from the coast. The fourth developed coastal algorithm, C2C UP4, which uses additionally the γ_{800} parameter from the ECMWF ERA5 model, provided similar results to the previous one, with rms values of 3.1 cm between 5 and 10 km from the coast and 3.3 cm up to 5 km from the coast. Thus, the inclusion of a dynamic γ_{800} input, alongside a dynamic SST, was not significantly impactful in coastal regions. These results are consistent with the results discussed in [8] for open-ocean algorithms.

To complete the analysis presented in Figs. 7–9, in Fig. 10, the results of the rms of the differences $\mathrm{WPD_{GNSS}} - \mathrm{WPD_{MWR}}$ are presented, computed in classes of 5 km width of distance from coast and classes of 5 cm width of a first WPD value from the ECMWF Op. Only the best results in each stage were selected for this analysis. To better understand the improvement of each approach, in Fig. 11, the differences of rms of the results presented in Fig. 10 are also presented.

Up to 10 km of distance from coast, the Op. 3I algorithm shows an rms of WPD differences of 4.5 cm and higher for the entire WPD range up to 40 cm. For these ranges of distance from coast and WPD, the improvement, relative to the last algorithm, of the UP3S0 open-ocean algorithm with modified inputs (O2C UP3S03) can reach 1 cm and higher values.

The improvement of the usage of a coastal algorithm with modified inputs (C2C UP2), relative to the UP3S0 open-ocean algorithm with the same modified inputs, is also in the order of

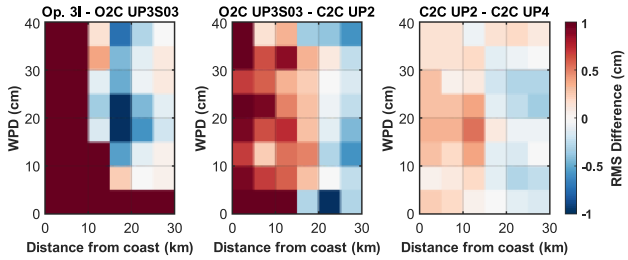

Fig. 11. Differences of rms values between the four WTC retrieval algorithms presented in Fig. 10, in classes of 5 km width of distance from coast and classes of 5 cm width of a first WPD value from the ECMWF operational model. Red colors are related to positive rms differences and blue colors to negative rms differences.

1 cm and higher values for distances from coast up to 20 km and the entire WPD range (center image in Fig. 11). An increase of the rms of WPD differences is observed for C2C UP2, relative to the prior algorithm, for distances from coast of 20 km and higher values. This increase is due to the fact that only Sentinel-3A SRAL/MWR measurements up to 20 km from the coast were used for the training of the coastal algorithms. Thus, C2C UP2 algorithm is not optimized for distances from coast equal or larger than 20 km.

For distances from coast up to 15 km, the addition of the SST and γ_{800} inputs in C2C UP4 algorithm improved the results, relative to C2C UP2 algorithm, for the whole range of WPD values, with a reduction of the rms up to 0.6 cm.

In Table III, the mean and rms of the differences $\mathrm{WPD_{GNSS}}$ – $\mathrm{WPD_{MWR}}$ are summarized for the various algorithms, for the first two classes of distance from coast.

In summary, the improvement, in terms of the rms reduction of the differences $\mathrm{WPD_{GNSS}} - \mathrm{WPD_{MWR}}$, of using modified inputs in the open-ocean UP3S0 algorithm (O2C UP3S03), relative to the Sentinel-3A MWR Op. 3I algorithm is of 5.3 cm between 5 and 10 km from coast and 11.8 cm up to 5 km from coast. The usage of coastal algorithms with unmodified inputs (C2C UP1) shows rms reductions, relative to the rms values of the Op. 3I algorithm, of 4.4 cm between 5 and 10 km from coast and 10.6 cm up to 5 km from coast. The combined strength of coastal algorithms with modified inputs (C2C UP2) improves further the rms values, with reductions of 5.9 cm between 5 and 10 km from coast and 12.6 cm up to 5 km from coast. The inclusion of external parameters to account for surface effects, namely the $\mathrm{SST_{skin}}$, further improves the rms values, with rms reductions relative to the rms values of the C2C UP2 algorithm, of 0.3 cm between 5 and 10 km from coast and up to 5 km from coast. Given the results presented in Table III, the inclusion of γ_{800} alongside the $\mathrm{SST_{skin}}$ (C2C UP4 algorithm) does not show a significant impact relative to the C2C UP3 algorithm.

B. Independent Assessment Against the ECMWF ERA5 Atmospheric Model

For the independent assessment against the ECMWF ERA5 atmospheric model, the totality of the Sentinel-3A SRAL/MWR measurements from the test dataset with distance from coast in the range 0–30 km were used. The database comprised a total of

TABLE III
MEAN AND RMS OF THE DIFFERENCES $\mathrm{WPD_{GNSS}} - \mathrm{WPD_{MWR}}$ FOR THE VARIOUS ALGORITHMS, FOR THE FIRST TWO CLASSES OF DISTANCE FROM COAST

Algorithm	Algorithm Description	0–5 km		5–10 km	
		Mean (cm)	RMS (cm)	Mean (cm)	RMS (cm)
Op. 3I	Open-ocean Sentinel-3A operational algorithm, MWR TBs and SRAL σ_0	–14.1	16.2	–7.4	9.2
O2C UP3S01	Open-ocean UP3S0 algorithm, MWR TBs modified by DistCoast and WPD classes, and unmodified SRAL σ_0	–1	6.2	–1.7	4.7
O2C UP3S02	Open-ocean UP3S0 algorithm, MWR TBs modified by LF and WPD classes, and unmodified SRAL σ_0	–1.9	4.9	–2	4.1
O2C UP3S03	Open-ocean UP3S0 algorithm, MWR TBs modified by LF and WPD classes, and SRAL σ_0 modified by DistCoast classes	–1.2	4.4	–1.5	3.9
O2C UP3WS	Open-ocean UP3WS algorithm, MWR TBs modified by LF and WPD classes, and 10-m U and V wind-speed components from the ERA5 model	–2.3	4.5	–2.1	4.1
C2C UP1	Coastal algorithm, unmodified MWR TBs and unmodified SRAL σ_0	–2.1	5.6	–2.3	4.8
C2C UP2	Coastal algorithm, MWR TBs modified by LF and WPD classes, and SRAL σ_0 modified by DistCoast classes	–0.7	3.6	–0.5	3.3
C2C UP3	Coastal algorithm, MWR TBs modified by LF and WPD classes, SRAL σ_0 modified by DistCoast classes, and $\mathrm{SST_{skin}}$ from the ERA5 model	–0.6	3.3	–0.5	3.0
C2C UP4	Coastal algorithm, MWR TBs modified by LF and WPD classes, SRAL σ_0 modified by DistCoast classes, and $\mathrm{SST_{skin}}$ and γ_{800} from the ERA5 model	–0.5	3.3	–0.4	3.1

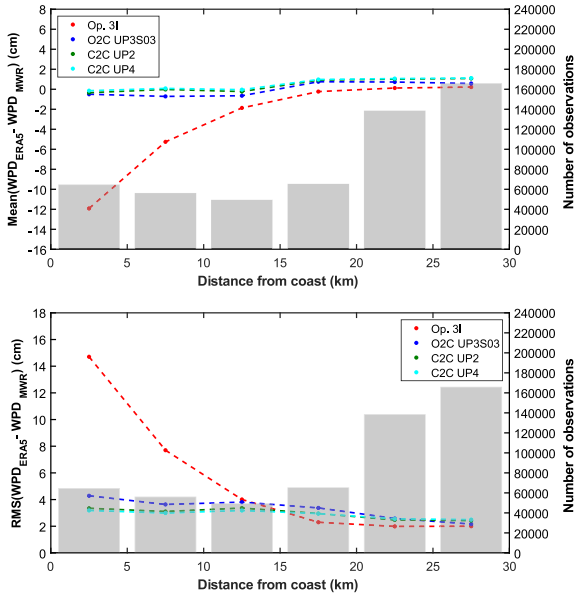

Fig. 12. Mean (top) and rms (bottom) of the differences $\mathrm{WPD_{ERA5}} - \mathrm{WPD_{MWR}}$, in classes of 5 km width of distance from coast, for the Sentinel-3A three-inputs MWR operational algorithm (Op. 3I), the UP3S0 algorithm with modified TBs and a modified σ_0 (O2C UP3S03), and the second and fourth developed coastal algorithms (C2C UP2 and C2C UP4, respectively). Grey bars represent the number of observations available in each class.

539 272 Sentinel-3A SRAL/MWR measurements. This second comparison serves as a complement to the assessment against GNSS stations presented in the last subsection, and, additionally, allows for a more broad and global assessment in regions without GNSS stations.

The mean and rms of the differences $\mathrm{WPD_{ERA5}} - \mathrm{WPD_{MWR}}$ are presented in Fig. 12, in classes of 5 km width of distance from coast, for a selected number of approaches presented in the last subsection.

The results of the mean and rms of the differences $\mathrm{WPD_{ERA5}} - \mathrm{WPD_{MWR}}$ agree with the same assessment results against GNSS stations. The best results were obtained with C2C UP2 and C2C UP4 algorithms, with the last algorithm presenting a slightly lower rms of WPD differences than C2C UP2 algorithm for the first three classes of distance from coast, up to 15 km. For C2C UP4, the rms of WPD differences is 3.2 cm between 10 and 15 km from the coast, 3.0 cm between 5 and 10 km from the coast, and 3.2 cm up to 5 km from the coast.

In Fig. 13, the differences of rms values of the results presented in Fig. 12 are presented, computed in classes of 5 km width of distance from coast and classes of 5 cm width of a first WPD value from the ECMWF Op. The results are very similar to those presented in Fig. 11.

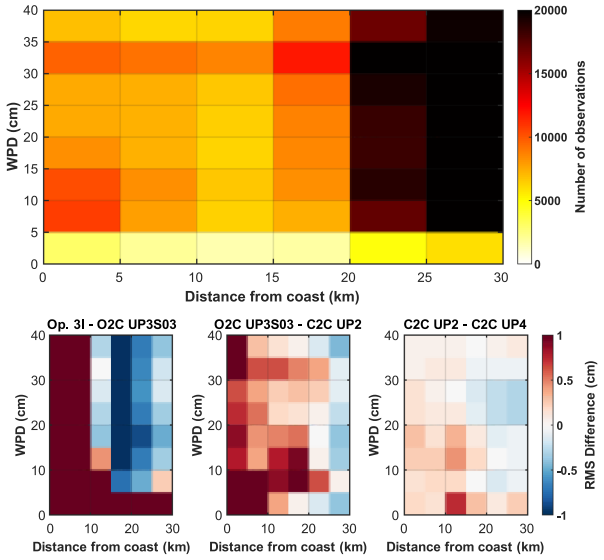

Fig. 13. Differences of rms values between the four WTC retrieval algorithms presented in Fig. 12, in classes of 5 km width of distance from coast and classes of 5 cm width of a first WPD value from the ECMWF Op. The top figure shows the number of observations for each image tile.

VI. Conclusion

The WTC retrieval over coastal regions is still a challenging task, mainly due to the land contamination in the radiometer TBs and, also related to this effect, due to the nonoptimization of the open-ocean geophysical retrieval algorithms over these transition surfaces.

This study aimed to improve the WTC over coastal regions for the Sentinel-3 mission, based on the dual-band MWR TBs and complementary parameters to account for surface effects. The use of the open-ocean UP3S0 algorithm with modified inputs significantly improved the retrieval errors in the WTC, relative to the Sentinel-3A MWR Op. 3I algorithm. Moreover, the developed coastal algorithms, with the same modified inputs, further improved the WTC retrieval errors.

A comparison against coastal and islands GNSS stations was performed, although such comparison is limited to the locations where such stations exist. Moreover, the comparisons are not collocated in space and time, thus, comparisons between MWR-derived WPD values against ZWD values derived from GNSS stations possess an inherent error derived from the noncollocation between both sources.

The best results were obtained with a five-inputs coastal neural network algorithm, with modified TBs, parametrized by classes of MWR LF and a first WPD value from the ECMWF Op., a modified SRAL σ_0, at Ku band, parametrized by classes of distance from coast, and the $\mathrm{SST}_{\mathrm{skin}}$ and γ_{800} parameters extracted from the ECMWF ERA5 atmospheric model. When compared to GNSS observations, the rms of the differences is 3.1 cm between 5 and 10 km from the coast and 3.3 cm up to 5 km from the coast. Moreover, the four-inputs version of the last algorithm, where the γ_{800} parameter is not considered, provided similar results, with rms values of 3.0 cm between 5 and 10 km from the coast and 3.3 cm up to 5 km from the coast.

For the Sentinel-3A Op. 3I algorithm, the rms of the differences for the same classes of distance from coast are 9.2 and 16.2 cm, respectively, leading to an rms reduction of 6.1 and 12.9 cm, respectively, with the proposed methodology. For the first uncontaminated class of distances from coast, between 15 and 20 km, the rms of the differences is 2.7 cm. The increased rms values for the first two classes of distance from coast, in the order of 0.6 cm higher, are due to land contamination effects, which are significantly reduced with the developed methods. All the results mentioned above are in line of agreement with the comparison against the ERA5 model.

Although significant improvements have been achieved, more work needs to be done to further reduce the retrieval errors and meet the requirements for coastal altimetry applications. Additionally, one can also benefit from technological improvements on the radiometer and altimeter sensors, which can aid for a more accurate WTC retrieval over coastal regions.

Acknowledgment

The authors would like to thank EUMETSAT for providing the Sentinel-3A data and the European Centre for Medium-Range Weather Forecasts and Copernicus Climate Change Service for providing the ERA5 atmospheric and surface fields.

References

[1] M. Ablain et al., "Uncertainty in satellite estimates of global mean sea-level changes, trend and acceleration," *Earth Syst. Sci. Data*, vol. 11, no. 3, pp. 1189–1202, Aug. 2019, doi: 10.5194/essd-11-1189-2019.

[2] M. J. Fernandes, C. Lázaro, and T. Vieira, "On the role of the troposphere in satellite altimetry," *Remote Sens. Environ.*, vol. 252, Jan. 2021, Art. no. 112149, doi: 10.1016/j.rse.2020.112149.

[3] J. Stum, P. Sicard, L. Carrere, and J. Lambin, "Using objective analysis of scanning radiometer measurements to compute the water vapor path delay for altimetry," *IEEE Trans. Geosci. Remote Sens.*, vol. 49, no. 9, pp. 3211–3224, Sep. 2011, doi: 10.1109/TGRS.2011.2104967.

[4] C. Donlon et al., "The copernicus sentinel-6 mission: Enhanced continuity of satellite sea level measurements from space," *Remote Sens. Environ.*, vol. 258, Jun. 2021, Art. no. 112395, doi: 10.1016/j.rse.2021.112395.

[5] S. J. Keihm, M. A. Janssen, and C. S. Ruf, "TOPEX/poseidon microwave radiometer (TMR). III. Wet troposphere range correction algorithm and pre-launch error budget," *IEEE Trans. Geosci. Remote Sens.*, vol. 33, no. 1, pp. 147–161, Jan. 1995, doi: 10.1109/36.368213.

[6] E. Obligis, L. Eymard, N. Tran, S. Labroue, and P. Femenias, "First three years of the microwave radiometer aboard Envisat: In-flight calibration, processing, and validation of the geophysical products," *J. Atmos. Ocean. Technol.*, vol. 23, no. 6, pp. 802–814, 2006, doi: 10.1175/JTECH1878.1.

[7] E. Obligis, A. Rahmani, L. Eymard, S. Labroue, and E. Bronner, "An improved retrieval algorithm for water vapor retrieval: Application to the Envisat microwave radiometer," *IEEE Trans. Geosci. Remote Sens.*, vol. 47, no. 9, pp. 3057–3064, Sep. 2009, doi: 10.1109/TGRS.2009.2020433.

[8] T. Vieira, M. J. Fernandes, and C. Lázaro, "An enhanced retrieval of the wet tropospheric correction for Sentinel-3 using dynamic inputs from ERA5," *J. Geodesy*, vol. 96, Apr. 2022, Art. no. 28, doi: 10.1007/s00190-022-01622-z.

[9] M.-L. Frery et al., "Sentinel-3 microwave radiometers: Instrument description, calibration and geophysical products performances," *Remote Sens.*, vol. 12, no. 16, 2020, Art. no. 2590, doi: 10.3390/rs12162590.

[10] T. Vieira, M. J. Fernandes, and C. Lázaro, "Independent assessment of on-board microwave radiometer measurements in coastal zones using tropospheric delays from GNSS," *IEEE Trans. Geosci. Remote Sens.*, vol. 57, no. 3, pp. 1804–1816, Mar. 2019, doi: 10.1109/TGRS.2018.2869258.

[11] R. Bennartz, "On the use of SSM/I measurements in coastal regions," *J. Atmos. Ocean. Technol.*, vol. 16, no. 4, pp. 417–431, Apr. 1999, doi: 10.1175/1520-0426(1999)016<0417:OTUOSI>2.0.CO;2.

[12] C. Desportes, E. Obligis, and L. Eymard, "On the wet tropospheric correction for altimetry in coastal regions," *IEEE Trans. Geosci. Remote Sens.*, vol. 45, no. 7, pp. 2139–2149, Jul. 2007, doi: 10.1109/TGRS.2006.888967.
[13] S. Brown, "A novel near-land radiometer wet path-delay retrieval algorithm: Application to the Jason-2/OSTM advanced microwave radiometer," *IEEE Trans. Geosci. Remote Sens.*, vol. 48, no. 4, pp. 1986–1992, Apr. 2010, doi: 10.1109/TGRS.2009.2037220.
[14] C. Lázaro, M. J. Fernandes, T. Vieira, and E. Vieira, "A coastally improved global dataset of wet tropospheric corrections for satellite altimetry," *Earth Syst. Sci. Data*, vol. 12, no. 4, pp. 3205–3228, 2020, doi: 10.5194/essd-12-3205-2020.
[15] C. Desportes, E. Obligis, and L. Eymard, "One-dimensional variational retrieval of the wet tropospheric correction for altimetry in coastal regions," *IEEE Trans. Geosci. Remote Sens.*, vol. 48, no. 3, pp. 1001–1008, Mar. 2010, doi: 10.1109/TGRS.2009.2031494.
[16] C. Donlon et al., "The global monitoring for environment and security (GMES) sentinel-3 mission," *Remote Sens. Environ.*, vol. 120, pp. 37–57, May 2012, doi: 10.1016/j.rse.2011.07.024.
[17] H. Hersbach et al., "The ERA5 global reanalysis," *Quart. J. Roy. Meteorol. Soc.*, vol. 146, no. 730, pp. 1999–2049, Jul. 2020, doi: 10.1002/qj.3803.
[18] H. S. Hopfield, "Two-quartic tropospheric refractivity profile for correcting satellite data," *J. Geophys. Res.*, vol. 74, no. 18, pp. 4487–4499, Aug. 1969, doi: 10.1029/JC074i018p04487.
[19] J. Saastamoinen, "Atmospheric correction for the troposphere and stratosphere in radio ranging satellites," in *The Use of Artificial Satellites for Geodesy*, vol. 15, S.W. Henriksen, A. Mancini, and B. H. Chovitz, Eds., American Geophysical Union, Jan. 1972, doi: 10.1029/GM015p0247.
[20] J. L. Davis, T. A. Herring, I. I. Shapiro, A. E. E. Rogers, and G. Elgered, "Geodesy by radio interferometry: Effects of atmospheric modeling errors on estimates of baseline length," *Radio Sci.*, vol. 20, no. 6, pp. 1593–1607, 1985, doi: 10.1029/RS020i006p01593.
[21] J. Kouba, "Implementation and testing of the gridded Vienna mapping function 1 (VMF1)," *J. Geodesy*, vol. 82, pp. 193–205, Apr. 2008, doi: 10.1007/s00190-007-0170-0.
[22] H. Hersbach et al., "ERA5 hourly data on pressure levels from 1979 to present," Copernicus Climate Change Service (C3S) Climate Data Store (CDS), 2018. Accessed: Mar. 6, 2023. [Online]. Available: https://cds.climate.copernicus.eu/cdsapp#!/dataset/reanalysis-era5-pressure-levels
[23] M. Miller, R. Buizza, J. Haseler, M. Hortal, P. Janssen, and A. Untch, "Increased resolution in the ECMWF deterministic and ensemble prediction systems," *ECMWF Newslett.*, vol. 124, pp. 10–16, 2010, doi: 10.21957/kyhds35r.
[24] J.-F. Pekel, A. Cottam, N. Gorelick, and A. S. Belward, "High-resolution mapping of global surface water and its long-term changes," *Nature*, vol. 540, pp. 418–422, Dec. 2016, doi: 10.1038/nature20584.
[25] H. Hersbach et al., "ERA5 hourly data on single levels from 1979 to present," Copernicus Climate Change Service (C3S) Climate Data Store (CDS), 2018. Accessed: Mar. 6, 2023. [Online]. Available: https://cds.climate.copernicus.eu/cdsapp#!/dataset/reanalysis-era5-single-levels
[26] The CEOS Database. Accessed: May 3, 2023. [Online]. Available: http://database.eohandbook.com/

Pedro Aguiar was born in Porto, Portugal, in 1993. He received the B.S. and M.S. degrees in surveying engineering, in 2017 and 2020, respectively, from the Faculty of Sciences, University of Porto, Porto, Portugal, where he is currently working toward the Ph.D. degree in surveying engineering with a focus on the wet tropospheric correction retrieval for satellite altimetry studies over homogeneous and transition surfaces.

His research interests include satellite radar altimetry and the exploration of external data sources for the retrieval of the wet tropospheric correction for satellite altimetry, namely global navigation satellite systems and atmospheric models.

Telmo Vieira was born in Mesquinhata, Baião, Portugal, in 1992. He received the B.S., M.S., and Ph.D. degrees in surveying engineering from the Faculty of Sciences, University of Porto (FCUP), Porto, Portugal, in 2013, 2015, and 2021, respectively.

He is currently working as a Junior Researcher with the FCUP. Since 2015, he has been a Researcher with the FCUP, when he joined the team of researchers that develop their work in satellite altimetry. He has been collaborating in several international research projects in which this team is involved, mostly funded by the European Space Agency. His research interests include satellite radar altimetry, global navigation satellite systems, and atmospheric models, in order to better modeling the effect of troposphere in the altimetric signals, mainly the wet troposphere over coastal and continental waters.

Clara Lázaro was born in Leça da Palmeira, Matosinhos, Portugal, in 1968. She received the B.S. degree in surveying engineering, the M.S. degree in remote sensing, and the Ph.D. degree in surveying engineering from the Faculty of Sciences, University of Porto (FCUP), Porto, Portugal, in 1993, 2003, and 2008, respectively.

From 1993 to 1994, she was a Research Trainee with the Astronomical Observatory, FCUP. From 1994 to 1999, she was a Research Trainee with the Tropical Research Institute, Geodesy Research Centre, Lisbon, Portugal. Since 2000, she has been a Staff Member with the FCUP, where she is currently an Assistant Professor with the Department of Geosciences, Environment and Spatial Plannings and the Director of the FCUP master's in surveying engineering. Her research interests include radar satellite altimetry, the development of methodologies for the improvement of the tropospheric corrections for use in satellite altimetry, and the application of satellite altimetry for ocean circulation and sea-level studies.

M. Joana Fernandes received the B.Sc. degree in surveying engineering from the Faculty of Sciences, University of Porto (FCUP), Porto, Portugal, in 1984, the M.Sc. degree in remote sensing from the University College London, London, U.K., in 1988, and the Ph.D. degree in remote sensing from the University of London, London, U.K., in 1993.

Since 1986, she has been a Staff Member with the FCUP and is currently an Associate Professor with Habilitation, teaching geodesy, hydrographic surveying, and remote sensing. She was the Director of the FCUP Ph.D. in surveying engineering and of the M.Sc. in remote sensing for several years. Over the last 20 years, her research interests include satellite altimetry in the following two main topics: 1) development of methodologies for improving the range and geophysical corrections required to derive accurate surface heights from satellite altimeter observations, with a focus on coastal and inland water regions and 2) satellite altimetry applications. Her research interests include the development of methods for retrieving the wet tropospheric correction and the sea state bias on satellite altimeter observations.